sustainability

MDPI

Article

Generating a Landslide Susceptibility Map Using Integrated Meta-Heuristic Optimization and Machine Learning Models

Tuba Bostan

Civil Engineering Department, Faculty of Civil, Yildiz Technical University, 34220 Istanbul, Türkiye; bostan@yildiz.edu.tr

Abstract: A landslide susceptibility assessment is one of the critical steps in planning for landslide disaster prevention. Advanced machine learning methods can be used as data-driven approaches for landslide susceptibility zonation with several landslide conditioning factors. Despite there being a number of studies on landslide susceptibility assessment, the literature is limited in several contexts, such as parameter optimization, an examination of the factors in detail, and study area. This study addresses these lacks in the literature and aims to develop a landslide susceptibility map of Kentucky, US. Four machine learning methods, namely artificial neural network (ANN), k-nearest neighbor (KNN), support vector machine (SVM), and stochastic gradient boosting (SGB), were used to train the dataset comprising sixteen landslide conditioning factors after pre-processing the data in terms of data encoding, data scaling, and dimension reduction. The hyperparameters of the machine learning methods were optimized using a state-of-the-art artificial bee colony (ABC) algorithm. The permutation importance and Shapley additive explanations (SHAP) methods were employed to reduce the dimension of the dataset and examine the contributions of each landslide conditioning factor to the output variable, respectively. The findings show that the ABC-SGB hybrid model achieved the highest prediction performance. The SHAP summary plot developed using the ABC-SGB model shows that intense precipitation, distance to faults, and slope were the most significant factors affecting landslide susceptibility. The SHAP analysis further underlines that increases in intense precipitation, distance to faults, and slope are associated with an increase in the probability of landslide incidents. The findings attained in this study can be used by decision makers to develop the most effective resource allocation plan for preventing landslides and minimizing related damages.

Keywords: landslides; machine learning; landslide susceptibility; artificial bee colony algorithm; model interpretability

check for updates

Citation: Bostan, T. Generating a Landslide Susceptibility Map Using Integrated Meta-Heuristic Optimization and Machine Learning Models. *Sustainability* **2024**, *16*, 9396. https://doi.org/10.3390/su16219396

Academic Editor: Maurizio Lazzari

Received: 15 September 2024
Revised: 21 October 2024
Accepted: 24 October 2024
Published: 29 October 2024

Copyright: © 2024 by the author. Licensee MDPI, Basel, Switzerland. This article is an open access article distributed under the terms and conditions of the Creative Commons Attribution (CC BY) license (https://creativecommons.org/licenses/by/4.0/).

1. Introduction

Landslides are among the most threatening geological disasters and can pose significant risks to peoples' lives and properties all over the world [1]. Particularly in mountainous and hilly regions, due to steep slopes, landslides may cause millions of economic losses by blocking transportation networks and causing utility interruptions [2–4]. Global records underline that nearly 2.2 million people are affected by landslides [5]. In the US, landslides cause billions of US dollar economic losses along with 50 casualties every year [6]. Over the past two decades, nearly 1500 landslide incidents were experienced in Kentucky alone [7]. Landslides not only cause the closure of roads but also disrupt utilities with interruptions and reduce the value of properties, with millions of US dollars of estimated economic losses occurring in Kentucky [8].

Many decision makers in governmental agencies tried to minimize the effects of landslides through proper planning and decision making [3]. Here, identifying the areas that are most susceptible to landslides can be regarded as an effective way of determining the most critical areas for early warning and resource allocation [9]. Landslide susceptibility mapping is the assessment of a specific region regarding their probability of landsliding

based on various criteria, such as geology, land use, slope, aspects, etc. [10]. Typically, machine learning methods can be used for the early diagnosis of the extent to which certain areas are prone to landsliding. Therefore, landslide susceptibility assessment using machine learning methods has become a prominent research direction for disaster prevention [11].

The pertinent literature on disaster prevention includes many studies on landslide susceptibility assessment. For example, Catani et al. [12] adopted the ensemble random forest (RF) method for developing a landslide susceptibility map of the Arno River Basin, Italy. The researchers included a variety of numerical and categorical variables and found that the dimension of the variables, scale of mapping, and training process affected the accuracy of the predictions. Similarly, Devi et al. [4] developed a machine learning-based landslide susceptibility assessment for Bhagirathi Valley, NW Himalaya. The researchers adopted several methods, such as random forest (RF), extreme gradient boosting (XGBoost), and k-nearest neighbor (KNN), and deduced that a greater part of the examined study area was classified as highly or very highly vulnerable zones to landsliding. Hong et al. [2] developed a decision tree (DT)-based ensemble model for the landslide susceptibility zonation of the Guangchang area, China. Using several variables such as slope, aspect, altitude, topographic wetness index, etc., the researchers concluded that the rotation forest model achieved the highest classification accuracy. Another ensemble-based machine learning approach for landslide susceptibility analysis was conducted by Kadavi et al. [3] in the Sacheon-myeon area in South Korea. They compared the performance of adaptive boosting (Adaboost), logitboost, multiclass classifier, and bagging based on twenty conditioning variables and achieved the highest prediction power while training the model with a multiclass classifier. Pourghasemi et al. [13] tested the performance of a generalized linear model, mixture discriminant analysis, boosted regression tree, and functional discriminant analysis for landslide susceptibility zonation in Fars Province, which covers 7% of Iran. They found that the most significant variables were the distance from the road, altitude, lithological units, and slope. By focusing on the China–Pakistan economic corridor region, Ullah et al. [14] developed a machine learning-based landslide susceptibility analysis using thirteen variables grouped into topographic, land cover, hydrological, geological, and meteorological categories. They identified that elevation, rainfall, lithology, slope, and land use were the most critical variables. Lv et al. [11] adopted the RF, support vector machine (SVM), and extreme gradient boosting (XGBoost) methods and focused on the Sichuan–Tibet region for a landslide susceptibility assessment. The researchers conducted an in-depth examination of the contributions of the variables as well as their interactions using the Shapley additive explanations (SHAP) method.

There are many other landslide susceptibility assessment studies adopting different methods with diverging perspectives [10,15–17]. However, the literature on landslide susceptibility assessment using machine learning methods is limited in several ways. The literature covers many powerful hyperparameter tuning algorithms devoted for different purposes, such as Optuna [18], genetic algorithm [19], particle swarm optimization [20], etc. However, none of the existing studies adopted one of the powerful metaheuristic optimization algorithms, namely artificial bee colony (ABC), to optimize the hyperparameters of the developed machine learning methods. The researchers considered a trial-and-error approach to tune the hyperparameters of the adopted methods. Second, only limited studies adopted one of the recently developed game theory-based feature examination algorithms, SHAP. The SHAP method not only investigates the weights of the conditioning factors but also presents which factors contribute to the prediction, how, and to which direction. Third, none of the existing studies considered the study area of Kentucky, US, for susceptibility zonation despite there being threatening records in the region.

Therefore, this study aims to develop a landslide susceptibility map of Kentucky, US, and examine the conditioning factors in detail. To achieve the objective of the research, four widely used machine learning methods from different machine learning families, such as artificial neural network (ANN), KNN, SVM, and stochastic gradient boosting (SGB), were adopted. The parameters of the methods were optimized using ABC, which is one

of the powerful optimization algorithms available. The dimension of the conditioning factors was also optimized using the permutation importance approach. Finally, the SHAP algorithm was utilized to examine the effects of landslide conditioning factors on the predictions. Overall, this research is expected to help decision makers develop the most effective resource allocation for landslide disaster prevention planning in Kentucky, US.

2. Materials and Methods

2.1. Research Framework

Machine learning, mainly relying on data-driven approaches, has emerged as one of the subsets of artificial intelligence applications. Conceptually, the modeling of sophisticated relationships among affective factors and the outcomes being affected by independent variables is carried out in the context of machine learning implementations. Given the intricate nature of nature-induced phenomena, these algorithms have been widely recognized by researchers to deal with complex challenges across the globe. Hence, this research aims to identify the regions with a likelihood of experiencing landslide events in the Kentucky River catchment due to constantly being subjected to the adverse impacts of such geo-hydrological hazards. In this respect, four different machine learning algorithms, each from different machine learning rationales, are employed. The major objective of the current research is to explore the performance of the SGB in landslide susceptibility attempts, while the model is benchmarked with three commonly adopted machine learning algorithms, namely ANN, SVM, and KNN. It is also worth noting that the selected machine learning methods encompass divergent internal hyperparameters that need to be diligently tuned in order to satisfy problem-specific objectives, better mimicking real-world conditions. Therefore, the ABC was integrated into each machine learning algorithm. Consequently, a total of four different predictive schemes were considered within the scope of this study, broadly assessing the performance of different data-driven approaches.

Among divergent train/test splitting strategies (e.g., 50/50, 60/40, 70/30, 80/20, and 90/10), the present research uses 70% and 30% for training and testing, respectively. Hence, this study allocates 70% of the data to the training set, while the remaining 30% is used as the blinded testing set. Additionally, within the present research, a rigorous 5-fold cross-validation method is employed to delineate the optimum hyperparameter sets during the optimization attempts. To make a fair comparison, this study takes various performance metrics into account, such as accuracy, precision, recall, F1-score, and the area under receiver operating curve (AUROC). The obtained results are visualized by means of the confusion matrices and AUROC plots. Along with several pre-processing (data encoding, data scaling, and dimension reduction) and processing (four different predictive frameworks) approaches, the SHAP algorithm is integrated as a post-processing approach to better reflect the effects of the variations observed within the predictors to the landslide susceptibility levels across the studied basin. Finally, based on the four different hybrid predictive schemes, susceptibility maps are generated with respect to the testing results attained for each hybrid model. The finalized map was provided and recommended for the model outperforming its counterparts concerning divergent performance evaluation criteria. The steps achieved within the scope of the current research are summarized using a pictorial representation in Figure 1.

2.2. Study Area

The present research focuses on the state of Kentucky as it contains a catchment that widely experiences landslide incidents. The corresponding catchment is the Kentucky River catchment, covering nearly 18,000 km^2 in surface area. Among the tributaries of the Kentucky River (such as the Red, Dix, Middle Fork, North Fork, and South Fork Kentucky rivers), the Red River is considered as the major river feeding the Kentucky main stream. The topography of the catchment ranges between 41 and 998 m above ocean level, while the climatic characteristics vary across the basin. For instance, mean annual temperature across the Kentucky River catchment is measured as 13 °C. The Kentucky River is a major source

of drinking water for approximately 700,000 people in the region, including residents of Lexington, Kentucky's second-largest city. Along with landslide events, the basin also suffered from other geo-hydrological disasters, such as floods. Such that, the river basin is prone to flooding, and efforts have been made to manage flood risks through various control measures and by maintaining healthy floodplains. Accordingly, the river has a series of 14 locks and dams constructed primarily in the early 20th century to facilitate navigation and help maintain water levels. The geographical location and the boundaries of the basin are depicted in Figure 2.

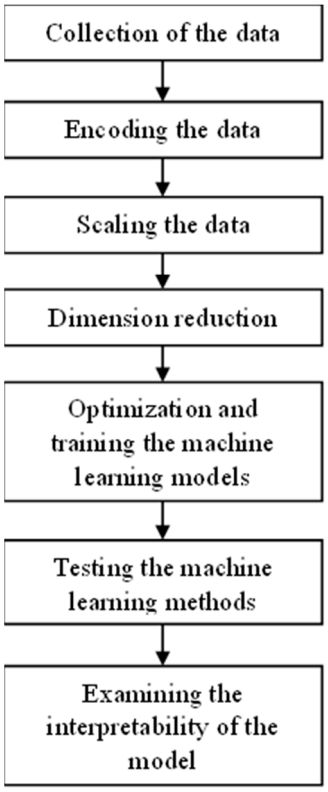


Figure 1. Research flowchart.

2.3. Landslide Inventory Mapping

Landslide inventory mapping is critical to not only understand the causal relationship of past events but also find the precautionary attempts made by the respective authorities. In line with this, potential incidents that can occur in the following periods can be simulated and the corresponding measures can be taken, guiding policymakers in the region to accommodate the practical applications in the field. Hence, inventories regarding such incidents have gained much more attention in recent years, especially concerning the impacts of remote sensing and the geographical information system (GIS), which are emerging technologies used to simulate nature-induced events, aiding in determining potential hazards and risks.

So, the present study obtained the records pertaining to the past landslide events from the USGS. The corresponding analysis resulted in a total of 726 landslide records considering the boundaries of the focalized domain. This study processed the corresponding dataset by utilizing different environments, such as Google Earth engine and ArcMap 10.3 [21]. In addition to the 726 recorded landslide points, the same number of artificial points were generated using ArcMap's "Create random points" command with the purpose of conducting fair assessments for landslide susceptibility mapping [22,23].

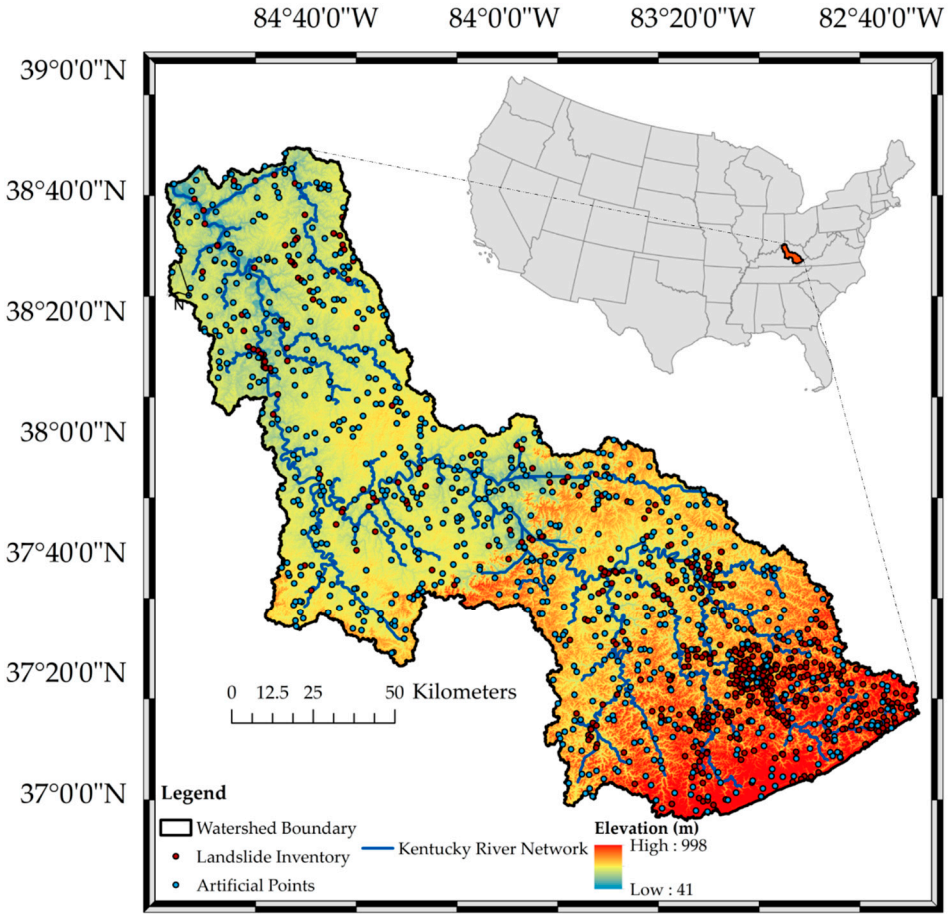


Figure 2. Kentucky River catchment.

2.4. Landslide Triggering Factors

Given their complex nature and intricate mechanics, landslide events are regarded as hard-to-predict phenomena using deterministic techniques. Instead, recent studies offer a more effective approach, such as data-driven techniques which are capable of simulating complex problems from a divergent point of view. Accordingly, key factors triggering the occurrences of landslide events are identified and used as independent variables to predict potential landslide-prone areas. To accomplish this overarching aim, machine learning algorithms are trained with the help of landslide conditioning factors and a target variable, while testing is processed in order to assess the validity of the trained models. The contribution of the utilized conditioning factors to predictions can also be determined, offering valuable insights into landslide simulation dynamics.

In this research, a total of 16 factors, e.g., aspect, curve number, distance to faults, distance to river, elevation, intense precipitation, land use/land cover, lithology, normalized difference vegetation index (NDVI), plan curvature, profile curvature, sediment transport index (STI), slope, stream density, topographic roughness index (TRI), and topographic wetness index (TWI), having the potential to influence the mechanisms underlying landslide formation, are investigated, as addressed in the literature. These factors were selected since they cover a variety of topographical (e.g., slope and elevation), geological (e.g., lithology and distance to faults), hydrological (e.g., stream density and TWI), and environmental (e.g., land use and NDVI) features of a specific area. These factors may affect the processes that are associated with the formation of landslides, such as the stability of soil and erosion. Hence, by incorporating a variety of factors, the multi-dimensional nature of landslides is addressed in a generic view.

The generated layers corresponding to these factors are presented in Figure 3. Also, the descriptive statistics of the utilized landslide conditioning factors are provided in Table 1. After conducting exploratory data analysis based on the statistics regarding the conditioning factors (Table 1), the application of some data pre-processing steps becomes a critical need. For instance, lithology and LULC were categorical variables with ranges of 2–7 and 11–90, respectively. Therefore, the elements in these categorical features should be represented in their numerical equivalences, which requires data encoding. Additionally, there are some factors with extreme values, and many numerical values are scaled in different formats. For instance, the minimum and mode of distance to faults attribute is 0, while the average and maximum values of the corresponding attribute are 13,815.06 and 47,021.40, respectively. In addition, while some features range between 0 and more than 10,000 (e.g., distance to faults, distance to river, and STI), some others range between 0 and 1 (e.g., intense precipitation, NDVI, and stream density). Therefore, to prevent machine learning models from being affected by the dataset with different intervals, data scaling is required as a pre-processing step. Finally, in order to enhance the performance of the models as well as improve computational efficiency, the appropriateness of the factors should be evaluated before the machine learning model is applied. Hence, dimension reduction should also be considered as a pre-processing step. These three pre-processing approaches are briefly summarized in the following sections.

Table 1. Descriptive statistics of the landslide conditioning factors.

Attribute	Mode	Min	Average	Max
Aspect	225.00	0.00	181.73	358.45
Curve Number	72.00	0.00	75.90	94.00
Distance to Faults	0.00	0.00	13,815.06	47,021.40
Distance to River	191.09	0.00	3006.56	12,358.40
Elevation	279.00	123.00	322.61	787.00
Intense Precipitation	1.00	0.00	0.50	1.00
Land Use/Land Cover	-	11.00	-	90.00
Lithology	-	2.00	-	7.00
NDVI	0.77	0.00	0.74	0.99
Plan Curvature	0.00	−1.31	−0.01	1.52
Profile Curvature	0.07	−1.85	0.11	2.72
Sediment Transport Index	0.00	0.00	35.55	18,880.00
Slope	3.45	0.27	14.00	43.85
Stream Density	0.00	0.00	0.13	0.37
Topographic Roughness Index	0.44	0.22	0.48	0.78
Topographic Wetness Index	7.39	3.85	7.05	20.20
Target	-	0.00	-	1.00

2.5. Data Encoding

Certain input parameters selected for an analysis may manifest in the form of categorical or text-based data. In such instances, data pre-processing becomes imperative to derive a meaningful representation of the dataset suitable for reliable, effective, and accurate processing by machine learning algorithms. Data encoding techniques are employed at this stage to facilitate the corresponding transformation. Data encoding therefore allows for converting categorical or text-based information into a numerical format compatible with machine learning algorithms. Within the literature, three widely accepted data encoding techniques are available for raw data preparation: label encoding, one-hot encoding, and target encoding. In this study, one-hot encoding is deliberately adopted due to its notable strengths, including its capacity to distinctly represent each category within the data, its facile handling of missing data, and its applicability to datasets of varying sizes. One-hot encoding operates by converting categorical data into a binary format, wherein unique categories are delineated into binary vectors, with each category corresponding to a distinct

binary column. In this research, one-hot encoding is used for transforming two categorical landslide conditioning factors, namely LULC and lithology.

Upon examining the data encoding techniques, one-hot encoding stands out as particularly advantageous, especially when dealing with categorical data characterized by nominal relationships. Nominal relationships imply that categories lack any inherent order or ranking, and each category holds equal significance within the dataset. One-hot encoding effectively addresses this by transforming categorical variables into binary vectors, wherein each unique category corresponds to its own binary column. This method ensures that all categories are distinctly represented without imposing any ordinal relationships among them, making it a useful choice for pre-processing categorical information in machine learning applications.

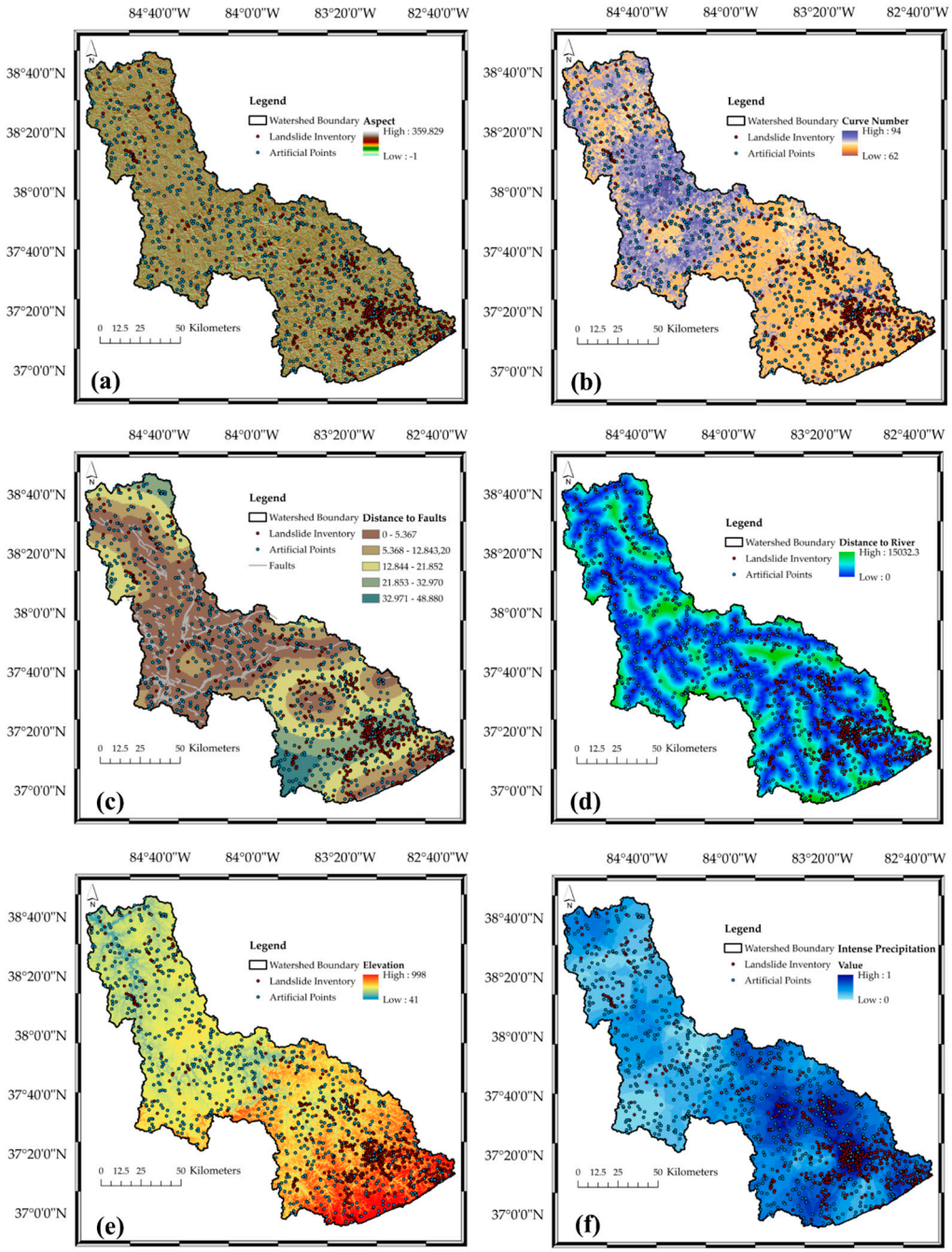


Figure 3. *Cont.*

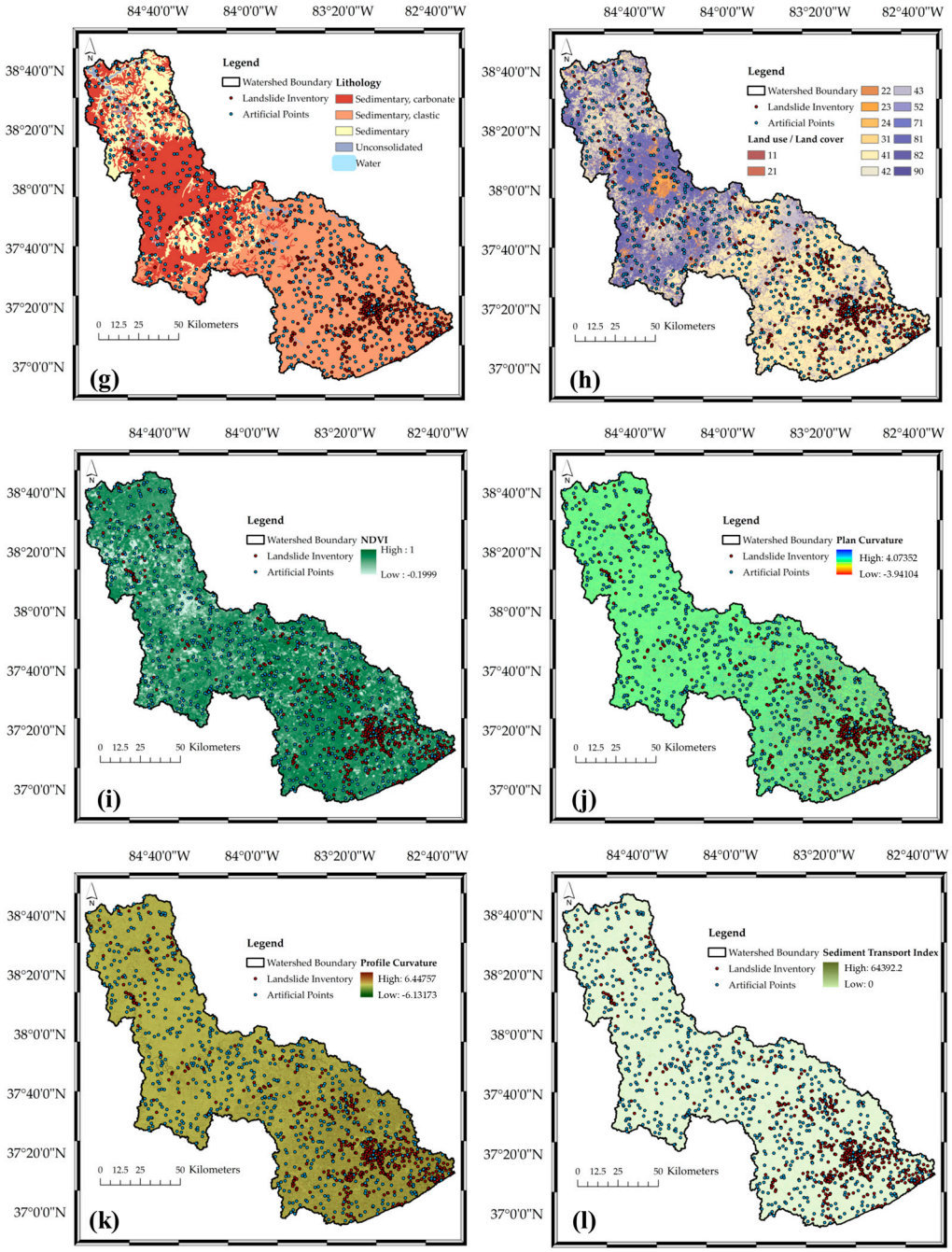


Figure 3. *Cont.*

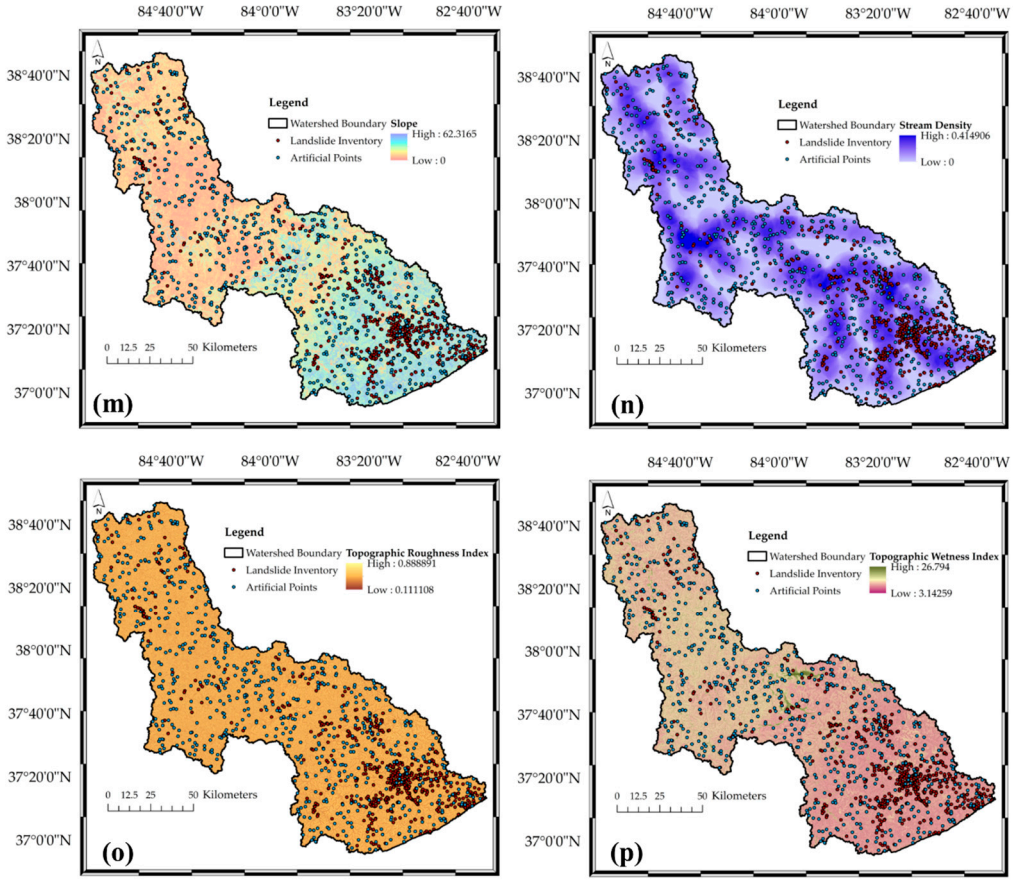


Figure 3. Attribute maps. (**a**) aspect, (**b**) curve number, (**c**) distance to faults, (**d**) distance to river, (**e**) elevation, (**f**) intense precipitation, (**g**) lithology, (**h**) land use/land cover, (**i**) NDVI, (**j**) plan curvature, (**k**) profile curvature, (**l**) sediment transport index, (**m**) slope, (**n**) stream density, (**o**) topographic roughness index, (**p**) topographic wetness index.

2.6. Data Scaling

Addressing challenges due to the presence of extreme values is often essential in order to inhibit potential disruption and misguiding in machine learning analysis. To overcome such issues, feature scaling techniques are adopted, and normalization (or standardization) of the utilized variables is performed to protect models influenced by the scale difference in a single variable. In this regard, divergent scaling mechanisms, e.g., min–max scaling (normalization), standardization (z-score scaling), robust scaling, and log transformation have been used by the research community. This study utilizes standardization owing to its several benefits, such as the fact that it is one of the most commonly adopted techniques and helps gradient boosting algorithms achieve faster convergence, ensuring features with larger scales do not dominate the model training process and allows all features to contribute equally to the model's learning process.

2.7. Dimension Reduction

In this study, a dimensional reduction approach is adopted to increase computational efficiency and enhance the performance of the predictive models. Hence, the present research specifically employs permutation importance, recognized as a robust and model-agnostic approach, particularly in scenarios with a high number of attributes [24,25]. In this sense, contributions of the predictors were assessed based on the computed permutation index values. Unlike other techniques embracing the leave-one-out scheme to perform sensitivity analysis, the working mechanism of permutation importance is based on substituting independent variables with noise datasets from the same distribution, allowing

for the nature of the utilized dataset to be procured. As a baseline model, due to its wide acceptance, this study adopts the random forest (RF) algorithm. A mean decrease accuracy approach is computed for each iteration through the incorporation of the RF algorithm into permutation importance. Hence, with regard to the accuracy alterations, a suitable ranking among the predictors is achieved.

The permutation importance technique mainly encompasses three consecutive stages. To achieve this, the identification of the original model's error (denoted as $e_{orig} = L(y, \hat{f}(X))$) is carried out at first (Stage 1). Then, a subsequent procedure depicted as follows is performed:

Stage 2.1. The attribute matrix (X_{perm}) is attained by permuting factor (j) in the original data (X).

Stage 2.2. The error ($e_{perm} = L(y, \hat{f}(X_{perm}))$) pertaining to the estimation of the permuted data is computed.

Stage 2.3. The permutation importance value is obtained through dividing the error obtained in Stage 2.3 (e_{perm}) by those obtained in Stage 1 (e_{orig}). In this way, the permutation importance ($FI_j = \frac{e_{perm}}{e_{orig}}$) is identified for each landslide conditioning factor.

Finally, the corresponding ranking is achieved as a result of ordering the attributes' importance (i.e., mean importance) in a descending manner (Stage 3).

2.8. Artificial Bee Colony Algorithm

A meta-heuristic optimization algorithm, artificial bee colony (ABC), was first introduced by Karaboga [26] to solve numerical optimization problems. The method is a population-based optimization technique, adopted by many researchers (e.g., [27–29]) to find a solution for multi-dimensional problems. ABC was inspired by the foraging behavior of honeybees. There are mainly seven steps of the ABC algorithm [30].

Step 1—The initial population: ABC creates an NF number of positions for food source and accordingly starts the searching procedure. A single artificial bee aims to determine the position of a food source. During the ABC algorithm process, NF remains constant.

Step 2—The employed bee phase: Every bee employed updates the most applicable optimization solutions by selecting a new potential source for food according to the neighborhood food source chosen initially. Then, from the previous solution ($x_{i,j}$), a new candidate, namely $u_{i,j}$, is created, as shown in Equation (1).

$$u_{i,j} = x_{i,j} + \phi_{i,j}\left(x_{i,j} - x_{k,j}\right) \tag{1}$$

where $\{k, i\} \in \{1, 2, \ldots, NF\}$, $j \in \{1, 2, \ldots, D\}$ are the indices chosen randomly, k is different than i, D is the size of the problem, and $\phi_{i,j}$ is a random number changing between -1 and 1. Therefore, bees are generated based on the power of the formerly explored sources. The potential candidate is replaced with the previous solution if the quality of food is higher than the latter; otherwise, the process continues with the earlier solution.

Step 3—The calculation of probability: When they come back to their hive, the employed bees share information about the food source with other bees. In this step, collective intelligence is generated by the algorithm for sharing critical information. The value of probability calculated by the algorithm affects the behaviors of the onlooker bees because these bees chose potential food sources according to the calculated probability. The value of probability in the ABC algorithm is calculated as

$$p_i = fit_i / \sum_{j=1}^{NF} fit_j \tag{2}$$

where fit_i is the value of the fitness for the food source i.

Step 4—The onlooker bee stage: As mentioned previously, onlooker bees choose a specific food source based on the p_i value calculated for the corresponding food source. In the ABC algorithm, Equation (1) is used to generate onlooker bees. Based on the nectar

available at the new location, a greedy approach is considered. Accordingly, onlooker bees update the location or maintain the previous solution.

Step 5—Updating the best food source location: After Step 4, the best food source location is identified. The following new best food source location is replaced with the old best food source location if the latter presents an equal or higher amount of nectar; otherwise, the process continues with the previous food source location.

Step 6—The scout bee stage: When the food source location x_i does not show any improvement based on the user-determined consecutive cycles, the bee abandons the solution x_i, which is replaced with a new food source location determined by the scout bee.

Step 7—The stop condition: The optimization of the ABC algorithm is finalized when the stop criteria determined by the user are met. The terminated optimized solution is presented to the user at the end of the optimization process.

It is worth mentioning that there are many hyperparameter tuning algorithms in the relevant literature. Some of these techniques are regarded as meta-heuristics, while others can be described as Bayesian optimization methods [18]. The ABC method has the ability to perform global search in the solution space. This provides an advantage, especially in complex hyperparameter optimization problems with many local minima. Additionally, with its parallel working feature, the ABC algorithm shows good results in complex and non-linear optimization problems. Therefore, among many powerful hyperparameter optimization techniques providing accurate outcomes for different problems, e.g., Optuna [31,32], Genetic Algorithm [19], and PSO [20], this study utilizes the ABC algorithm.

2.9. Machine Learning

This study adopts four machine learning algorithms for landslide susceptibility mapping, namely ANN, KNN, SVM, and SGB. This study considers the trade-off between the number of hyperparameters optimized and the computational expense. Hyperparameter optimization is generally important for improving algorithm performance. However, testing numerous combinations with too many hyperparameters consumes more time and resources, which extends the optimization process and requires more computational power. Therefore, using fewer hyperparameters narrows down the hyperparameter space of the model, leading to faster results. However, this approach also has some limitations; in some cases, using fewer parameters may not fully unlock the model's potential. Hence, finding the right balance is important in achieving optimal model performance. The hyperparameters, parameter ranges, steps, and total candidates examined in each method are provided in Table 2. The following paragraphs present a brief description of each method.

Table 2. Hyperparameter ranges in ML methods.

ML Method	Hyperparameter	Range	Step	Total Candidates
ANN	Activation Function	Relu, TanH, Logistic	-	600
	Momentum	0.5–1	0.05	
	Number of Hidden Neurons	5–100	56	
KNN	Metric	Euclidean, Manhattan, Chebyshev, Minkowski	-	200
	Number of Neighbors	0–50	1	
SVC	Kernel Function	Polynomial, Radial Basis, Sigmoid	-	600
	Gamma	2^{-15}–2^{3}	-	
	C	0–200	10	
SGB	Number of Trees	0–500	50	500
	Learning Rate	0.0025–0.015	0.0025	
	Maximum Depth	0–10	1	

ANN is one of the machine learning methods that mimics the human brain in a systematic way such that biological cells such as neurons are modeled in the ANN structure [33]. Inputs in a typical ANN structure refer to the information presented to the model, and weights are the extent to which the information is provided to a neuron. The net function indicates the computational procedure for calculating the net input for the neuron, while the activation function processes the net input and weights so that the output can be calculated. There are two major stages in the learning process of ANN: feed forward and back propagation. In the feed forward stage, the weights are evaluated, and the output of the model for a sample provided is achieved. In back propagation, based on the prediction and expected results, weights are updated. The main role of back propagation is to minimize the sum of error squares via training. In the ANN model, the activation function, momentum, and the number of hidden neurons are optimized. The activation function enhances the model's learning performance in non-linear relationships, while momentum and the number of hidden neurons accelerate the training process by improving optimization and determine the model's complexity and learning capacity, respectively.

The KNN algorithm is a sample-based machine learning algorithm. In this algorithm, the nearest neighbor to the data sample is identified according to the k value [34]. There are mainly five steps covered by the KNN algorithm outlined in the sequel: (1) the value of k is identified; (2) the distances between the target data and the others are calculated; (3) the distances are considered in the ascending order, and the neighborhoods are specified based on the closest distance in which the data with the smallest distance is regarded as the 1st neighbor while the data with the largest is the nth neighbor (if n is the total number of a data sample); (4) the number of k nearest neighbor classes is collected; and (5) the most commonly observed neighbor class is selected based on the majority voting. It is worth noting that the metrics, such as Euclidean, Manhattan, Minkowski, and Chebyshev, used for the calculation of the distance between observations may also vary depending upon the type of variables, i.e., continuous and categorical. For instance, using the Euclidean distance for continuous variables is suitable, while the Manhattan distance is a good match with the categorical variables [35]. In this study, the metric and the number of neighbors were considered as optimized KNN model parameters. The metric defines the distance between neighbors, while the number of neighbors indicates how many neighbors will be considered when assigning a sample to a class. More neighbors can make the model more general, but too many neighbors can cause decision boundaries to become overly flat.

SVM is a vector-based machine learning method that is based on structural risk minimization principle via statistical leaning theory [36]. In this method, a hyperplane, which indicates a line dividing a class of data points, is identified. However, a perfect hyperplane cannot be attained in non-linear problems. In other words, the error is allowed in the learning process, and the hyperplane with the lowest error is obtained. At the end, the hyperplane with the maximum margin and minimum error is obtained, namely optimum hyperplane [37]. In many real-life problems with non-linear datasets, a linear hyperplane cannot be formed, and kernel functions are usually used for enhancing the model's accuracy [38]. There are several kernels, such as radial basis function, sigmoid function, and polynomial function. Since the selected kernel significantly impacts the performance of the model, the kernel is also considered as one of the parameters to be tuned in the parameter tuning process. As for the SVC hyperparameters, the kernel function, gamma, and the C parameter were optimized. The kernel function is the mathematical function used by SVC to find the classification boundaries in the data. Additionally, the gamma parameter determines the influence of the kernel function on the model. The C parameter is related to classification errors. A high C value increases model accuracy, while a low value decreases it.

The present research utilized the SGB technique among different techniques in tree-based machine learning algorithms. While the literature features a range of tree-based methods, including bagging and boosting techniques, XGBoost (version 2.1.2) has seen widespread use due to its extensive functionality. However, SGB was chosen in this research

for its simplicity and ease of implementation. Additionally, SGB incorporates bootstrap aggregation by using random subsets of data in each iteration, helping to mitigate overfitting. Another key factor considered in the analysis was computational efficiency. Since SGB processes only a random portion of the data during each iteration, it is computationally more efficient. This makes SGB a faster alternative to XGBoost, particularly when working with smaller datasets. Hence, SGB is also regarded as one of the powerful tree-based modeling methods. Gradient boosting helps improve the performance of the model as well as to decrease computational load. At each iteration, additive models are generated by fitting base learner in terms of least squares in the GBDT technique [39]. To compute the captured information, GBDT uses each data instance in every feature, which makes the trade-off between performance and efficiency a critical concern [40]. Additionally, GBDT algorithm might be subjected to overfitting, especially if a powerful regularization is not employed in the iteration stage [41]. Therefore, Friedman [39] proposed the SGB method, which includes randomness into the machine learning procedure, different from the GBDT algorithm. Hence, instead of the full samples, random sub-samples are attained from the training set for fitting the base learners. The SGB contains three different hyperparameters (number of trees, learning rate, and maximum depth) optimized within this study. A higher number of trees generally makes the model stronger, but it also increases the risk of overfitting, creating a trade-off. The learning rate determines how much each tree contributes to the model's performance. The selection of maximum depth should be handled carefully. Similar to the number of trees, a higher value allows the model to learn more details but also increases the risk of overfitting.

2.10. Performance Evaluation

Predictive accuracy of machine learning algorithms with the specific purpose to make classification attempts is determined using divergent performance measurement metrics. In this sense, four major statistical measures are fundamentally utilized. The corresponding measures are as follows:

(1) True Positive (TP): This is the measure of the number of correctly classified instances in the positive label.
(2) True Negative (TN): This is the measure of the number of correctly classified instances in the negative label.
(3) False Positive (FP): This is the measure of the number of incorrectly classified instances in the negative label.
(4) False Negative (FN): This is the measure of the number of incorrectly classified instances in the positive label.

With the utilization of the four above-mentioned measures, different indicators can be identified. Among these indicators, accuracy is one of the widely accepted, whereas precision and recall can also be computed. Accuracy is simply defined as the ratio of the total number of correctly classified landslide points divided by the total number of landslide points, including both landslide inventory and artificially generated points. Hence, accuracy is formulated as follows:

$$Accuracy = \frac{TP + TN}{TP + FN + FP + TN} \quad (3)$$

Likewise, the ratio of the number of correctly classified positive landslide points (TP) to the summation of the positively classified landslide points (i.e., both TP and FP) provides the precision metric, as depicted in Equation (4).

$$Precision = \frac{TP}{TP + FP} \quad (4)$$

Unlike precision, recall concentrates on false positive landslide points, and it is the ratio of correctly classified positive landslide points (TP) to the summation of the correctly

classified positive landslide points (TP) and false negative landslide points (FN), which Equation (5) demonstrates:

$$Recall = \frac{TP}{TP + FN} \tag{5}$$

Along with the accuracy, precision, and recall, the current study evaluated the classification performance of the machine learning models used with regard to the F1-score, which combines the information that comes from both precision and recall. Hence, the F1-score is described as the harmonic mean of the precision and recall and is computed as follows:

$$F1 - score = \frac{2 \times Precision \times Recall}{Precision + Recall} \tag{6}$$

In order to perform a comprehensive evaluation of the landslide predictions, this research further analyzed the impact of the area under receiver operating curve (AUROC) on the model performances. The AUROC is computed based on a graph representation that encompasses information related to the false positive rate (x-axis) and true positive rate (y-axis). The formulation of the AUROC is illustrated as follows:

$$AUC = 1 - \frac{1}{m^+ m^-} \sum_{x^+ \epsilon\ M^+} \sum_{x^- \epsilon\ M^-} \left(\left(f(x^+) < f(x^-) \right) + \frac{1}{2} \left(f(x^+) = f(x^-) \right) \right) \tag{7}$$

where m^+ and m^- are positive and negative instances, M^+ and M^- are sets of all positive and negative instances, and x^+ and x^- are positive and negative classes, respectively. In the formula, $f(x)$ denotes the outcome of prediction model sample x. It is worth mentioning that the AUROC varies between 0.5 and 1, where 0.5 depicts the worst performance, while 1 shows that the landslide predictions are perfectly matched with the landslide incidents observed.

Cohen's Kappa is one of the indicators that shows the consistency of a prediction model's classification results. In addition, this indicator takes into account the probability of random agreement in addition to classification performance. A Kappa value approaching 1 means perfect agreement, 0 indicates no agreement, and negative values indicate even greater disagreement [42].

$$\kappa = \frac{p_0 - p_e}{1 - p_e} \tag{8}$$

where P_0 depicts the observed proportion of agreement between the observed and predicted classes, while P_e is the expected proportion of agreement by chance.

The average area under the precision–recall curve (AUC-PR) represents the area under the precision–recall curve. A high AUC-PR value indicates that the model has a high ability to correctly predict positive classes.

2.11. Shapley Additive Explanations

In the pertinent body of literature regarding machine learning applications, artificial intelligence techniques are often criticized in terms of their lack of capability to explain physical mechanisms behind the predictions due to their black-box nature. However, divergent efforts have been devoted to overcoming the corresponding challenge recently. For instance, the SHAP algorithm fostered by Shapley [43] based on the game theory has recently been used in order to enhance the interpretability of the applied artificial intelligence techniques by the research community. As it is a model-agnostic methodology, the SHAP algorithm has received significant attention, and thus, it has been incorporated into various machine learning techniques for numerous purposes, including environmental, geological, hydrological, etc., applications. The SHAP method is capable of handling problems with sophisticated relationships among its ingredients, making it a useful approach to understand the interactions among the independent variables governing the occurrences of different nature-induced phenomena.

The SHAP algorithm aids in obtaining the contributions of the predictors identified through the Shapley values that are computed based on the coalition game theory. In this sense, consider the machine learning model $g(\mathrm{a})$ with predictors $a = (a_1, a_2, \ldots, a_i)$, where i denotes the number of independent variables. This model, then, can be represented as follows:

$$g(\mathrm{a}) = h(\mathrm{a}') = \phi_0 + \sum_{i=1}^{N} \phi_i a_i' \tag{9}$$

In this formulation, a_i' represents the simplified independent variable, and $h(\mathrm{a}')$ is the explanatory model. Here, N refers to the number of landslide instances utilized in the simulations, and ϕ_0 varies based on whether the predictions increase or decrease in subsequent steps, and it is the constant term when all the predictors are absent. This equation provides a unique solution that maintains local accuracy, ensuring that the function's output is the sum of feature attributions and that no importance is given to missing features. Furthermore, it ensures consistency, meaning that increasing the impact of a feature does not reduce the attribution given to that feature [44]. Based on this information, the Shapley values denoted by ϕ_i can be obtained using the following equation:

$$\phi_i(g, \mathrm{a}) = \sum_{\mathrm{y}' \subseteq \mathrm{a}'} \frac{|\mathrm{y}'|!(N - |\mathrm{y}'| - 1)!}{N!} \left[g_a(\mathrm{y}') - g_a(\mathrm{y}' \setminus i) \right] \tag{10}$$

where $|\mathrm{y}'|$ is the number of non-zero entities in the subset y' that meets the specified condition with $\mathrm{y}' \subseteq \mathrm{a}'$.

Shapley values obtained can also be used in various ways (such as summary plots, dependence plots, etc.), allowing to achieve visually appealing explanations. In this research, SHAP summary plots were used to visually reflect the contributions of the landslide conditioning factors to the landslide susceptibility simulations. In the summary plot, the variations in the predictors can also be observed to further extend the interpretability of the constructed AI-based predictive framework.

3. Results

This section presents the major findings of the current study. Accordingly, dimensional reduction outcomes using the permutation importance technique are provide in Section 3.1. The results regarding the configuration of machine learning algorithms during training and validation processes are summarized in Section 3.2, while the performances of the established models are assessed with regard to the testing set and the generated final landslide susceptibility map based on the results obtained using the best-performed model are presented in Section 3.3.

3.1. Dimensional Reduction Results

In this study, a total of 16 different landslide conditioning factors were considered. Given the employed one-hot encoding scheme for categorical variables (i.e., lithology and land use/land cover), the total number of inputs taken into account in the predictions was 33, which limits the computational efficiency of the machine learning applications. Hence, the present research employed permutation importance to identify the key independent variables, primarily contributing to the prediction of landslide-prone regions. Due to the widespread usage of integrated PI and random forest (RF), this study incorporated the traditional tree-based RF algorithm into the PI determinations. The results obtained through this integrated framework are presented in Figure 4. It can be seen in the figure that, with the highest mean importance value, intense precipitation (also known as heavy rainfall) has the most significant impact on the landslide susceptibility predictions. In addition, one can observe in Figure 4 that the probability of intense precipitation is followed by two distinct LU/LC classes, i.e., LU/LC (22) and LU/LC (21), which reflect the presence (or non-existence) of developed–low-intensity and developed–open-space areas, respectively (https://www.mrlc.gov/data/legends/national-land-cover-database-class-

legend-and-description, accessed on 14 September 2024). Also, slope yielded one of the highest mean importance values, illustrating the augmented impact of slope on determining landslide-prone regions. At fifth and sixth places, the distance to faults and distance to river criteria are ranked, respectively, with mean importance values between 0.01 and 0.02. Similarly, LU/LC (41) and LU/LC (81) showed significant potential to have an impact on the estimation of landslide-prone areas, which represent deciduous forest areas dominated by trees generally greater than 5 m tall, and greater than 20% of total vegetation cover and pasture/hay areas of grasses, legumes, or grass–legume mixtures planted for livestock grazing or the production of seed or hay crops, typically on a perennial cycle, respectively. It is worth noting that the threshold aiding to eliminate the conditioning factors posing limited contribution to the predictions was set to 0. Therefore, most of the sub-classes of both lithology and LU/LC were excluded from the decision framework. Consequently, the number of predictors was reduced to 20, helping sustain the computational efficiency of the established hybrid predictive models. Hence, the following predictions were carried out concerning the predictors with mean importance values greater than 0.

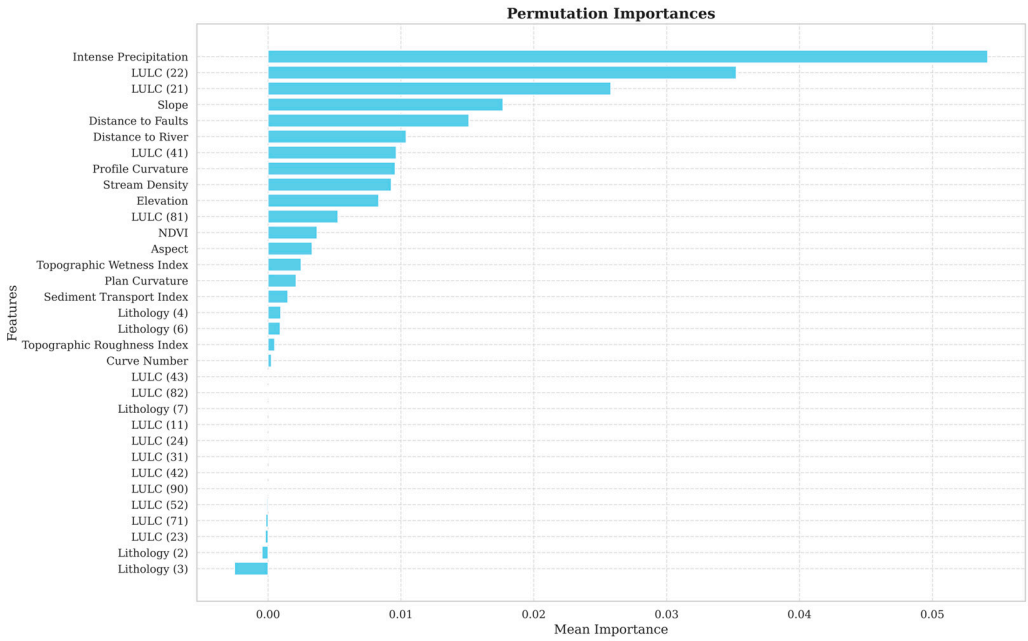


Figure 4. Permutation importance results to decrease the model dimension.

3.2. Training and Validation Results

In this research, a comprehensive performance comparison scheme is created with the adoption of four different machine learning algorithms (i.e., ANN, KNN, SVM, and SGB), each hybridized with the mate-heuristic hyperparameter tuning strategy, namely ABC. Binary classifications were performed for identifying landslide-prone regions in the Kentucky River basin. To obtain the best representative parameter set for the ML applications, the ABC algorithm was integrated, and the internal parameters of the utilized models were determined. Within the ANN applications, three different hyperparameters (namely activation function, momentum, and number of hidden neurons) were scanned in a search space encompassing a total of 600 candidates. Among three options (i.e., ReLu, TanH, and logistic), the ABC algorithm highlighted the ReLU as an activation function. In addition, the optimum values for the momentum and number of hidden neurons were found to be 0.95 and 35, respectively. The comparative analysis further revealed the limited effectiveness of the ABC-ANN technique with regard to both computational load and predictive accuracy since the corresponding model not only showed the highest duration but also the lowest mean training accuracy in hyperparameter tuning processes.

The KNN structure with a relatively smaller number of hyperparameters compared to its counterparts was also configured by the ABC. To carry this out, four different distance metrics (i.e., Euclidean, Manhattan, Chebyshev, and Minkowski) and 50 different numbers of neighbors (from 1 to 50) were scanned, resulting in a total of 200 combinations. However, distinct from the conventional grid search algorithm that is based on the trial of all parameter sets to find the ideal solution, the ABC algorithm yielded a faster convergence in a total of 793 s. As a result of the computations with respect to accuracy, which was chosen as the objective function, the distance metric and number of neighbors were attained as Manhattan and 13, respectively. The results pertaining to the hybrid use of the ABC and KNN (ABC-KNN model) showed a mean training accuracy of 0.8302, which shows that it outperforms both the ABC-ANN and ABC-SVM models. The ABC-SVM hybrid model ranked third concerning both the computational cost and predictive capability with a duration of 1056 s and an accuracy of 0.8260, respectively (Table 3). Among three commonly utilized kernel functions (namely Polynomial, Radial Basis, and Sigmoid), this research found the RBF as optimal, and the gamma and penalty (C) parameters were identified as 0.00195 and 80, respectively.

Table 3. Comparison of optimization results.

Hybrid Model	Duration (s)	Mean Training Accuracy	Optimum Hyperparameters
ABC-ANN	1229	0.8126	Activation function: ReLu Momentum: 0.95 Number of hidden neurons: 35
ABC-KNN	793	0.8302	Metric: Manhattan Number of neighbors: 13
ABC-SVM	1056	0.8260	Kernel: RBF Gamma: 0.00195 C: 80
ABC-SGB	825	0.8737	Number of trees: 100 Learning rate: 0.01 Maximum depth: 9

From the tree-based ML family, this research sought the assessment of the SGB technique in landslide susceptibility modeling attempts. Similar to the other ML techniques, the SGB was also subjected to the ABC algorithm to find the optimal configuration with a total of 500 candidate solutions. In this hyperparameter adjustment, the number of trees, learning rate, and maximum tree depth, ranging between 0 and 500, between 0.0025 and 0.015, and between 0 and 10, respectively, were optimized. Consequently, the ABC model resulted in an optimal value of 100 for the number of trees, 0.01 for the learning rate, and 9 for the maximum depth of the trees. It is especially worth highlighting that the hybrid ABC-SGB model is the best option due not only to its lowest computational load but also the mean training accuracy provided. In a total of 825 s, the ABC-SGB model outperformed its counterparts, revealing that it has the fastest convergence to the optimal solution, and among four hybrid models, it yielded the strongest predictive ability with the highest objective function value. Still, concerning the complex structure of such methodologies and their black-box nature, the performance of hybrid models configured through the meta-heuristic ABC was validated using the blinded testing sets. The major outcomes of the predictions made with respect to the testing set are provided in the following section.

3.3. Testing Results and Respective Landslide Susceptibility Mapping

The configured hybrid ML models in the training and validation phases were further subjected to the testing set to finalize the performance assessment scheme. In this regard, various performance evaluation indices, including accuracy, precision, recall, and F1-score, were computed for each model. The respective outcomes are summarized in Table 4. The table reveals that the ABC-SGB model is the best-performing model according to the predictions based on the blinded testing set. Although the highest predictive performance

with respect to the accuracy metric is obtained through both the ABC-SGB and ABC-SVM models with a value of 0.7681, the other performance indices illustrate the superiority of the ABC-SGB model over other hybrid techniques. In line with this, the F1-score was calculated as 0.7802, while the precision and recall values were obtained as 0.7812 and 0.7801 through the ABC-SGB, respectively. This model was followed by the ABC-SVM model with the same accuracy but lower precision, recall, and F1-score values of 0.7697, 0.7681, and 0.7680, respectively. It is interesting to note that, although the ABC-KNN model showed superior performance in training over the ABC-SVM model, its ability to predict the instances sustained in the blinded testing set was lower compared to the ABC-SVM model. Similar conclusions can also be made for the comparison of the ABC-ANN and ABC-KNN models such that despite the predictive success of the ABC-KNN model with regard to the training set among hybrid models, this model is ranked fourth due to its limited capability to simulate the landslide and non-landslide instances falling within the blinded testing set. Since the comparison of ML models is generally conducted concerning testing sets as they are sustained as blinded to reflect real-world conditions, one can conclude that the ABC-KNN model demonstrated the lowest performance with a precision of 0.7610, a recall of 0.7608, and a 0.7609 F1-score.

Table 4. The classification reports of the hybrid ML models.

		Performance Measures					
Set	**Hybrid Model**	**Accuracy**	**Precision**	**Recall**	**F1-Score**	**Kappa**	**AUC-PR**
Training	ABC-ANN	0.8126	0.8126	0.8196	0.8126	0.6251	0.7518
	ABC-KNN	0.8302	0.8302	0.8302	0.8301	0.6604	0.7703
	ABC-SVM	0.8260	0.8262	0.8260	0.8260	0.6520	0.7690
	ABC-SGB	0.8737	0.8604	0.8602	0.8603	0.8136	0.8692
Testing	ABC-ANN	0.7657	0.7679	0.7657	0.7655	0.5320	0.6251
	ABC-KNN	0.7608	0.7610	0.7608	0.7609	0.5216	0.7082
	ABC-SVM	0.7681	0.7697	0.7681	0.7680	0.5367	0.7200
	ABC-SGB	0.7681	0.7812	0.7801	0.7802	0.7802	0.7438

Table 4 further shows the Kappa and area under the precision–recall curve (AUC-PR) values. Accordingly, the most powerful method for the testing set regarding the Kappa statistics was again the ABC-SGB model (Kappa: 0.7802), followed by the ABC-SVM (Kappa: 0.5367), ABC-ANN (Kappa: 0.5320), and ABC-KNN (Kappa: 0.5216) models. Similar conclusions can also be drawn for the AUC-PR metric, such that the ABC-SGB model was the most powerful hybrid model, followed by the ABC-SVM, ABC-KNN, and ABC-ANN model, with AUC-PR values of 0.7438, 0.7200, 0.7082, and 0.6251, respectively.

To further support the obtained outcomes, the present study also provided the confusion matrices, allowing for the predictive aptitude of the configured ML models specific to landslide and non-landslide instances' predictions to be assessed (Figure 5). Similarly, the ABC-SGB model outperformed its counterparts with the highest percentage of correctly classified landslides (1) and non-landslides (0). For instance, the ABC-SGB model (Figure 5d) correctly predicted 75.94% of the regions that experienced landslide incidents correctly, while this hybrid framework also captured 82.18% of the non-landslide points. In other words, the ABC-SGB model predicted only 24.06% and 17.82% of the landslide and non-landslide events incorrectly. In contrast, the ABC-ANN model provided higher accuracy for predicting non-landslide events with a percentage of 80.20% (Figure 5a) compared to landslide events with 73.11% accuracy.

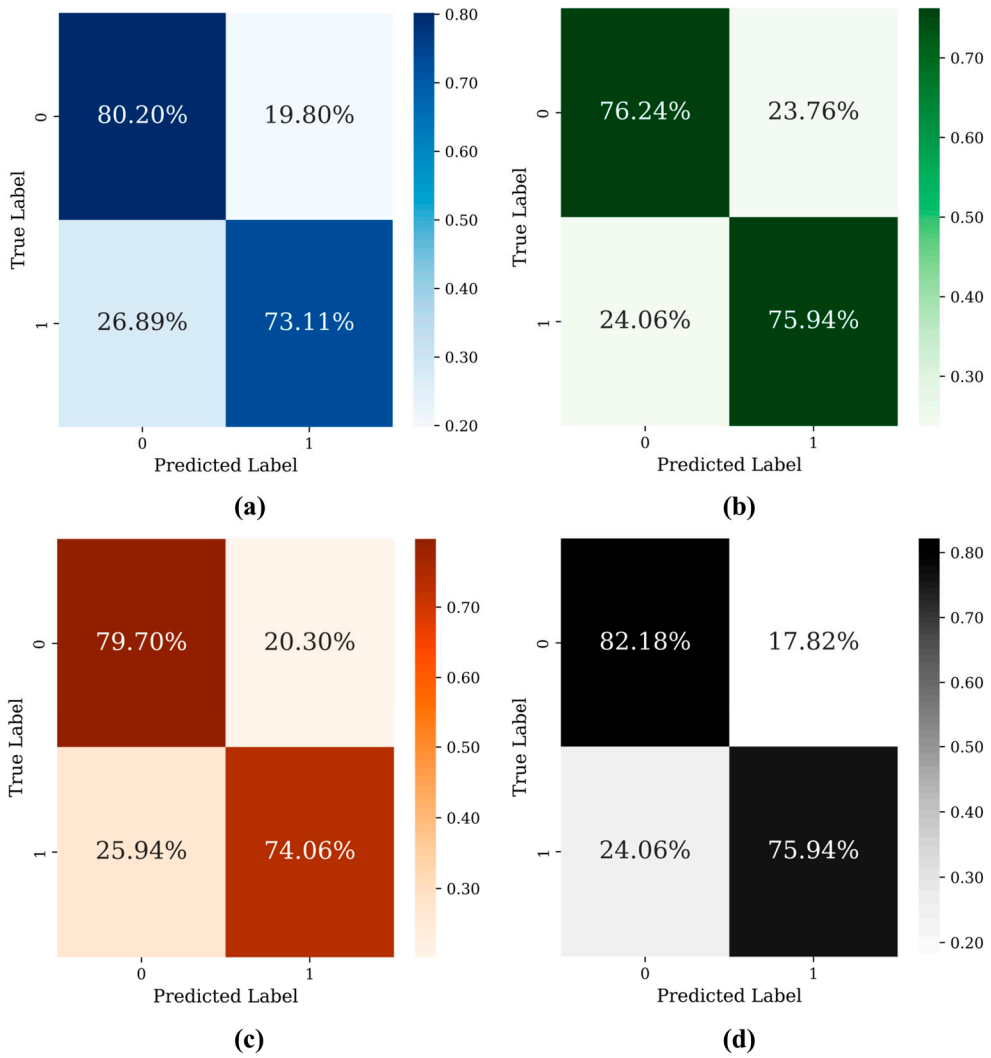


Figure 5. Confusion matrices of the hybrid ML algorithms based on the testing set: (**a**) ABC-ANN, (**b**) ABC-KNN, (**c**) ABC-SVM, and (**d**) ABC-SGB.

Compared to the ABC-ANN model, one can see the superiority of the ABC-KNN model (Figure 5b) with the ability to simulate 75.94% of landslide events (compared to 73.11%) correctly. In disaster-related studies, since the major objective is to identify disaster-prone locations to provide assistance to decision makers and policymakers for fostering mitigation measures, accurately predicting regions with a likelihood of such incidents is of paramount importance (compared to non-landslide regions). In this context, the ABC-ANN and ABC-SVM models showed relatively limited capability to accurately predict the regions that experienced landslides (1 concerning the binary classification) with values of 73.11% (Figure 5a) and 74.06% (Figure 5c), respectively. Although the ABC-KNN model underestimated the non-landslide locations, it provides significant insights regarding the determination of areas that have the potential to experience such disasters. Overall, it is again worth noting that, despite slight differences in performance comparisons achieved considering different metrics, the computational efficiency of the ABC-SGB model with lesser processing time need to be highlighted, making it an effective algorithm to simulate the landslide susceptibility conditions. Additionally, ABC-SGB model outperformed the other methods in detecting both landslide and non-landslide areas.

Besides divergent performance assessment metrics, the generated AUROC plots are provided within the scope of the current research (Figure 6). The reason for conducting such an additional attempt is the widespread acceptance of the AUROC, especially in

binary classification analysis. Similar to the previous evaluations, the ABC-SGB model outperformed its counterparts with AUROC values of 0.952 and 0.866 for the training and testing sets, respectively, making it the most robust predictive modeling alternative for landslide susceptibility mapping. In contrast, the ABC-ANN, ABC-KNN, and ABC-SVM models achieved AUROC values of 0.898, 0.908, and 0.904 for the training set, while they yielded AUROC values of 0.862, 0.861, and 0.856, for the testing set, respectively. The radar plots provided in Figure 7 illustrate the comparison of different models using Cohen's Kappa, accuracy, and AUC-PR. The findings show a clear distinction between the ABC-SGB model and other hybrid models for both the training and testing sets.

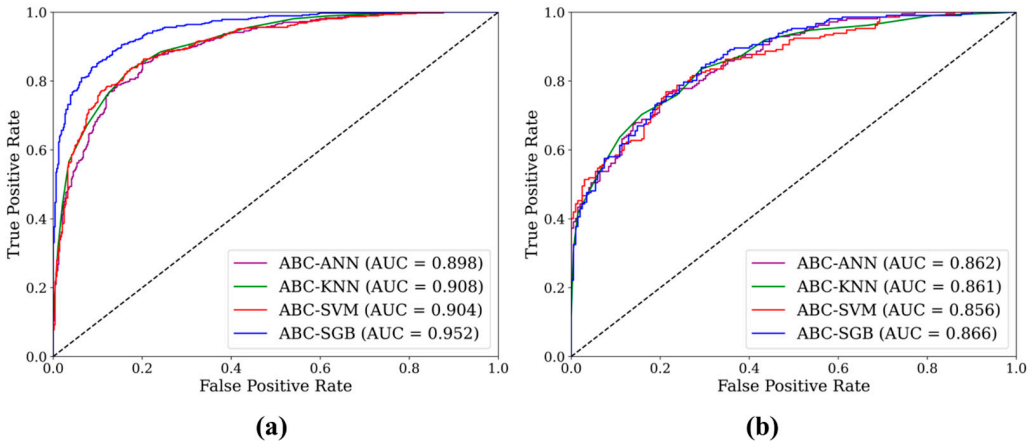


Figure 6. The ROC plots of the hybrid ML models based on the (**a**) training set and (**b**) testing set.

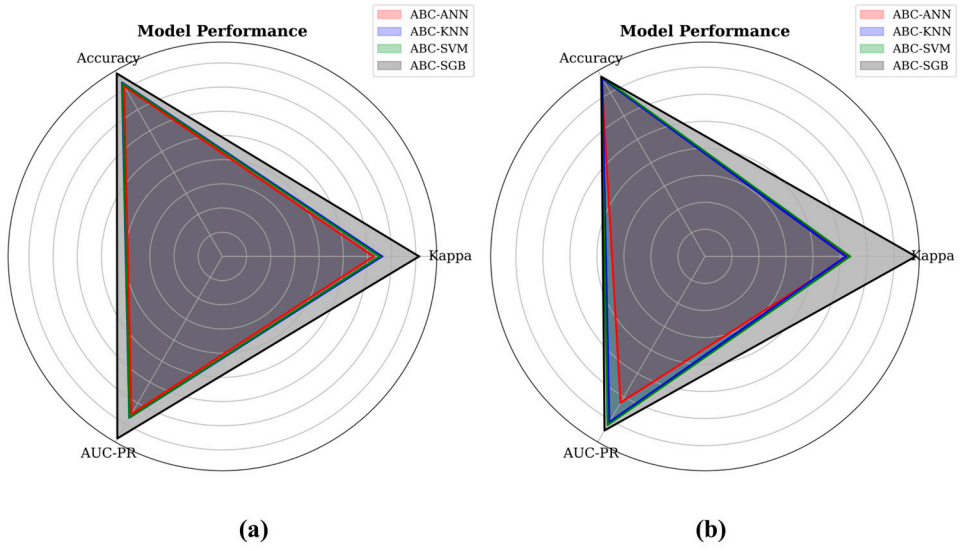


Figure 7. Radar plots of the hybrid ML models based on the (**a**) training set and (**b**) testing set.

According to the results obtained with respect to the testing set using the ABC-SGB hybrid model, a landslide susceptibility map is generated for the Kentucky River basin (Figure 8). To divide the susceptibility level to landslide events, Jenks natural break, which is one of the most commonly used optimization-based clustering methods, was used. Using this technique, the catchment was divided into five distinct classes, namely very low, low, moderate, high, and very high. The likelihood of experiencing landslide events in regions falling into the *very low* cluster was calculated to be 0.201 at most (out of 1), while a *low* likelihood is represented by a probability between 0.202 and 0.364. Regions having *moderate* potential to be subjected to landslide events have a probability between 0.365 and 0.531. Consequently, *high* and *very high* clusters refer to the likelihood of landslide events between

0.532 and 0.663 and between 0.664 and 1, respectively. Furthermore, area percentages with regard to each susceptibility cluster were computed for the region of interest. Associatively, as depicted in Figure 8, 33.4% of the interested area posed *very low* susceptibility, and domains located at mid-part and in the vicinity of the downstream showed *very low* susceptibility. Similarly, regions that have a *low* likelihood of being subjected to landslide incidents are positioned in a mid-part (a relatively smaller area compared to the very low cluster) and close to the downstream (a larger area compared to its counterparts) and cover 20.4% of the entire catchment. *Moderate* susceptibility is observed in 21.5% of the Kentucky River basin in which the corresponding regions are located in the regions with a relatively closer distance to the upstream and the northwest of the basin. In addition, areas with *high* and *very high* susceptibility to landslide incidents are positioned in the southern part of the basin, generally corresponding to higher elevations characterizing slopy properties (Figure 3e,m). These areas cover 14.7% and 10.0% of the basin, respectively. Along with the impact of elevation and slope, the potential to receive intense precipitation has a significant impact on the obtained findings as it is the most influential criterion according to the permutation importance. Accordingly, the corresponding regions (as illustrated in Figure 3f) corroborate the areas posing high and very high susceptibility to landslides.

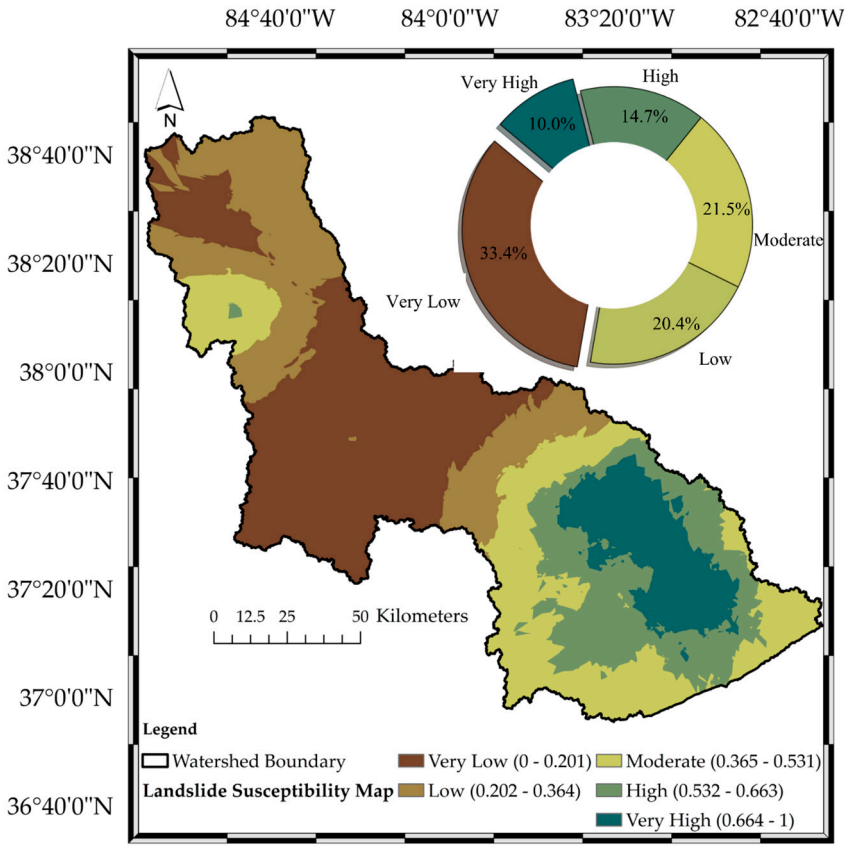


Figure 8. Landslide susceptibility map using ABC-SGB hybrid model.

4. Discussion

In this research, to increase the interpretability of the obtained findings, the SHAP algorithm was incorporated into the hybrid model, which enabled the highest predictive success [45], as recommended by researchers [42]. Hence, the ABC-SGB model was used to identify the contribution of the conditioning factors to the landslide events' predictions. Also, the five most contributing attributes are presented through a SHAP force plot in Figure 9. The SHAP force plot addresses the bold value (i.e., 0.60), which highlights the

model's score for an observation. Higher scores and lower scores lead the machine learning models to predict 1 and 0 in a binary classification problem. Additionally, the red bars increase the score, while the blue bars decrease the score. Hence, the figure illustrates that the area focused on in Figure 9 is predicted as a landslide point due to its high slope, intense precipitation, and land cover type of LULC (21). The findings are in line with the existing literature as researchers highlighted the role of intense precipitation and high slope as contributing conditions of landsliding [46].

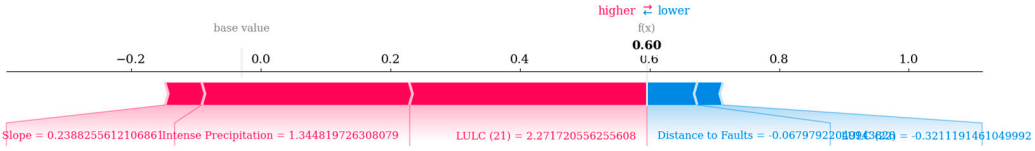


Figure 9. A SHAP force plot with regard to the best-performing SGB model.

The SHAP summary plot results are also presented in Figure 10 in which the attributes placed on the y-axis on the left-hand side of the figure are ordered from top to bottom based on their importance levels. The dark red points on the figure show that the actual values of the corresponding predictors converge to their higher values, while the dark blue points show the opposite. In addition, the points positioned on the right-hand side of the SHAP summary plot illustrate that the region tends to experience landslide incidents (coded as 1), whereas the points on the left-hand side indicate that these instances contribute to the decreasing trend in the likelihood of being subjected to landslide hazards. In this sense, the potential to receive intense precipitation events is highly influential in experiencing landslide events as this attribute is positioned at top, and the higher the probability of experiencing heavy meteorological incident in regions, the higher the likelihood of the occurrence of landslide events. This outcome can be supported with the generated layer in Figure 3f, which demonstrates the conglomeration of past landslide points on the regions that previously received intense precipitation (dark blue areas). Also, Camera et al. [46] recognized the significance of the inclusion of intense rainfall in landslide susceptibility mapping studies and found that an increase in rainfall values above a certain threshold results in an increase in the susceptibility of regions to landslide incidents. Likewise, Araújo et al. [47] considered that extreme rainfall events are of critical importance in terms of assessing the physical processes for landslide triggering, highlighting the importance of including rainfall regimes' in the identification of landslide susceptibility levels.

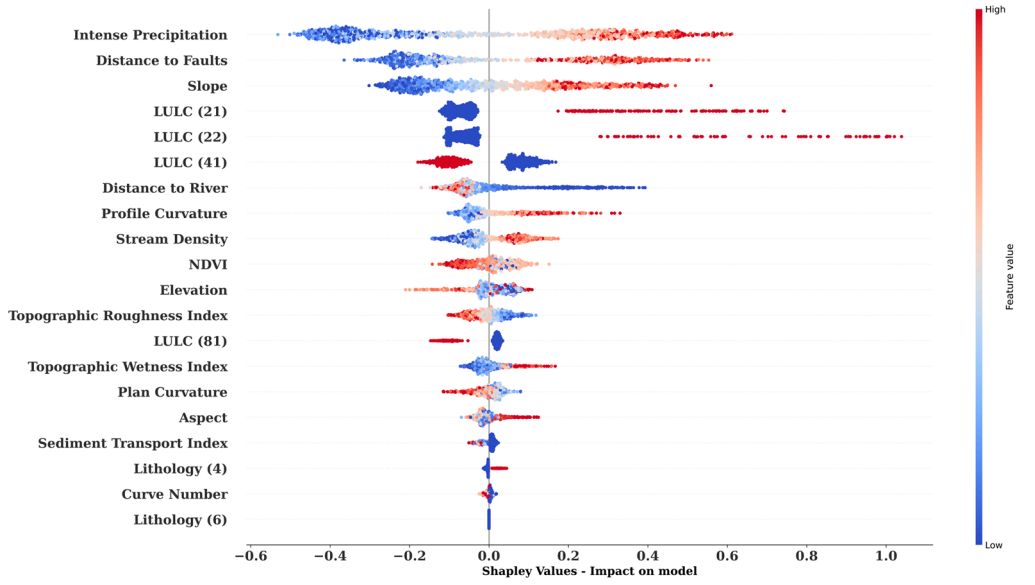


Figure 10. A SHAP summary plot with regard to the best-performing SGB model.

From another view, the present study found that the distance to faults criterion plays the second most important role in landslide susceptibility predictions. In line with this conclusion, Qi et al. [48] emphasized that the distance to coseismic faults is one of the most determinant factors with regard to the evaluation of landslides' spatial distributions. Although the results obtained within this study reveal that there is a positive correlation between the distance to faults and the likelihood of occurrence of landslide events, the corresponding outcome poses contradictory evidence compared to some of the past research. For instance, Zhao and Zhao [49] put forward that as the distance to fault increases, the likelihood of a landslide gradually decreases. On the other hand, Cui et al. [50] took nine different factors into account in order to investigate their impacts on the spatial variability of shallow landslides, and based on the Bayesian probability method used in this work, the researchers highlighted the positive correlation between the distance to faults and landslide occurrences. This unique distinction between not only the findings of this research and the pertinent literature but also among different studies existing in the literature can be associated with region-specific properties. Furthermore, the slope factor effectively reflecting the physical relationships between landslide and topographical units [51] was found to be the third most contributor to landslide simulations for the Kentucky River basin. Figure 10 further shows that the increase in slope instability has significant potential to increase the landslide susceptibility of regions, which corroborates the existing body of knowledge highlighting that unstable slopes are prone to the occurrence of landslides, especially in conjunction with the impact of extreme rainfalls and seismic activities [52,53].

The SHAP analysis also illustrated the impact of certain land use/land cover classes to landslide susceptibility predictions. For instance, the summary plot produced based on the ABC-SGB hybrid model shows that three classes of LULC, namely LULC (21), LULC (22), and LULC (41), have the fourth, fifth, and sixth highest impacts on the predictions performed. Among these three classes, the presence of the first two increases the likelihood of experiencing landslide events in the region, while the latter contributes to the preservation of areas against landslide hazards. It is worth mentioning that LULC (21) matches up to regions consisting of areas with minimal impervious surfaces, usually under 20%. The corresponding result can be attributed to various factors such that while areas posing the characteristics of LULC (21) are primarily vegetated and have low impervious surfaces, the type of development often associated with these areas with the anthropogenic impacts might disturb the natural landscape and soil structure, leading to an increase in the susceptibility to landslides. In a similar manner, the presence of the LULC (22) class referring to developed/low intensity areas with nearly 20% to 49% impervious surfaces can alter natural water drainage and increase surface runoff, which can lead to soil saturation and destabilization, particularly in areas prone to landslides. Moreover, another class of land use/land cover characterizing deciduous forests with deep-rooted trees, i.e., LULC (41), provides stability to the soil by reinforcing it and reducing the likelihood of erosion and landslide hazards. This fact broadly supports the outcome of the SHAP analysis revealing that the presence of such land use characteristics reduces the potential of experiencing landslides. However, it is especially worth mentioning that the risk of landslides may still be heightened despite the presence of vegetation if the forest is located on steep slopes or in areas with loose or unstable soils. Finally, the SHAP summary plot depicts that these factors were followed by the distance to river, profile curvature, stream density, NDVI, and so on, and interestingly, certain classes of the lithology (e.g., classes 4 and 6) have a limited impact on the determination of landslide-prone regions in the Kentucky River basin.

5. Conclusions

A landslide susceptibility assessment is a critical step in determining the areas that are prone to landslide risk. This study developed a machine learning-based landslide susceptibility assessment for the Kentucky River basin, US. Four widely used machine learning methods, ANN, KNN, SVM, and SGB, were trained, and the parameters of each method were optimized using the ABC algorithm. Hence, the major novelty of this research

is the integration of the ABC algorithm in four widely used machine learning methods for improving model accuracy and enhancing the generalizability of the captured best hyperparameters. Therefore, the performance of four hybrid models, namely ABC-ANN, ABC-KNN, ABC-SVM, and ABC-SGB, were compared. The contributions of the parameters were assessed using a recent and powerful method, SHAP. The main conclusions derived from this study can be listed as follows:

(1) The ABC-SGB model performed the best with a mean training accuracy of 0.8737 in which the optimization process lasted 825 s. The same model also achieved the highest performance for the testing set such that the F1-score, precision, recall, and AUROC values were calculated to be 0.7802, 0.7812, 0.7801, and 0.866, respectively. Therefore, the proposed ABC-SGB model can be used confidently to determine the areas most susceptible to landslides.
(2) A Jenks natural break analysis was conducted to identify the level of susceptibility to landsliding in Kentucky, and the results show that 10.0%, 14.7%, and 21.5% of the entire catchment were determined as very highly, highly, and moderately susceptible to landslide incidents.
(3) The SHAP analysis results show that intense precipitation, the distance to faults, slope instability, LULC (21), LULC (22), and LULC (41) were the most significant factors affecting the occurrence of landslides in the region. An in-depth analysis further shows that an increase in intense precipitation, distance to faults, slope instability, LULC (21), and LULC (22) are associated with an increase in the probability of landslide occurrence. Conversely, an increase in LULC (41) is associated with a decrease in the probability of landslide occurrence.

Even though many methods were applied, and a comprehensive point of view is provided, there are still some limitations in this research. For example, although this research compared the performance of widely used machine learning algorithms, there are other powerful methods, such as deep neural networks, Naïve Bayes, logistic regression, and decision trees. In particular, a tree-based method comparison might be an intriguing research direction since this study found the SGB algorithm, one of the tree-based algorithms, to be the most powerful algorithm. Here, the performance of the RF, XGBoost, Adaboost, and extra trees algorithms can be compared with the SGB algorithm. Additionally, there are other powerful optimization methods, such as Optuna, genetic algorithms, and particle swarm optimization. A comparative future study on metaheuristic optimization algorithms might therefore be a proper research direction. In addition, despite the trade-off between the number of hyperparameters and computational expense being considered in this study, other hyperparameters of machine learning methods can also be optimized in a future study. Additionally, this study used the SHAP algorithm to enhance the interpretability of the developed model. Still, there are other approaches that help improve the explainability of machine learning methods, such as local interpretable model-agnostic explanations and partial dependence plots. Therefore, with their pros and cons, explainable artificial intelligence approaches can be compared in a future study to show the dynamics of landslides in more detail. Another critical research direction can be related to the comparative performance of machine learning methods on different study areas, as a study area comparison was not carried out by these researchers. Hence, a future study can compare the performance of machine learning methods in different study areas for landslide susceptibility to ensure the generalizability of the developed models. Finally, this research focused on the development of a machine learning model for landslide susceptibility mapping rather than developing a framework to minimize the occurrence of landslide events. Therefore, a machine learning-based framework addressing specific risk mitigation measures can be a proper direction for future research.

This study has several practical implications. First, local authorities can use the generated landslide susceptibility map to specify the areas at risk of landsliding, which may help develop more effective land use planning and infrastructure development. Additionally, the most significant landslide conditioning factors, as well as their impacts on landslide

occurrence, were captured from an explainable data-driven machine learning approach (i.e., SHAP) in contrast to a survey-based examination of the factors. Therefore, local authorities and related stakeholders can be informed with the proposed model as data-driven models can yield highly accurate prioritizations. This may help find the most critical risk management approaches, eventually reducing landslide-related disasters. Even the use of an interpretable machine learning approach (i.e., SHAP) can convince local authorities and policymakers of the validity of the proposed model as traditional machine learning methods are usually criticized to be black-box models. Finally, by identifying the most susceptible areas with a highly accurate data-driven approach, risk monitoring and early warning systems can be focused on these areas, which can enhances effectiveness and efficiency in resource allocation. Overall, this study and potential future research directions can help decision makers develop the most effective means for managing catchments that are susceptible to landslides.

Funding: This research received no external funding.

Institutional Review Board Statement: Not applicable.

Informed Consent Statement: Not applicable.

Data Availability Statement: Publicly available datasets were analyzed in this study.

Conflicts of Interest: The author declares no conflicts of interest.

References

1. Maurizio, L.; Maria, D. A Multi Temporal Kernel Density Estimation Approach for New Triggered Landslides Forecasting and Susceptibility Assessment. *Disaster Adv.* **2012**, *5*, 100–108.
2. Hong, H.; Liu, J.; Bui, D.T.; Pradhan, B.; Acharya, T.D.; Pham, B.T.; Zhu, A.X.; Chen, W.; Ahmad, B. Bin Landslide Susceptibility Mapping Using J48 Decision Tree with AdaBoost, Bagging and Rotation Forest Ensembles in the Guangchang Area (China). *CATENA* **2018**, *163*, 399–413. [CrossRef]
3. Kadavi, P.R.; Lee, C.W.; Lee, S. Application of Ensemble-Based Machine Learning Models to Landslide Susceptibility Mapping. *Remote Sens.* **2018**, *10*, 1252. [CrossRef]
4. Devi, M.; Gupta, V.; Sarkar, K. Landslide Susceptibility Zonation Using Integrated Supervised and Unsupervised Machine Learning Techniques in the Bhagirathi Eco-Sensitive Zone (BESZ), Uttarakhand, Himalaya, India. *J. Earth Syst. Sci.* **2024**, *133*, 131. [CrossRef]
5. Anderson, M.G.; Holcombe, E. *Community-Based Landslide Risk Reduction*; The World Bank: Chicago, IL, USA, 2013; ISBN 978-0-8213-9456-4.
6. Mirus, B.B.; Jones, E.S.; Baum, R.L.; Godt, J.W.; Slaughter, S.; Crawford, M.M.; Lancaster, J.; Stanley, T.; Kirschbaum, D.B.; Burns, W.J.; et al. Landslides across the USA: Occurrence, Susceptibility, and Data Limitations. *Landslides* **2020**, *17*, 2271–2285. [CrossRef]
7. NCEI National Centers for Environmental Information. Available online: https://www.ncei.noaa.gov/ (accessed on 14 September 2024).
8. Crawford, M.M.; Dortch, J.M.; Koch, H.J.; Killen, A.A.; Zhu, J.; Zhu, Y.; Bryson, L.S.; Haneberg, W.C. Using Landslide-Inventory Mapping for a Combined Bagged-Trees and Logistic-Regression Approach to Determining Landslide Susceptibility in Eastern Kentucky, USA. *Q. J. Eng. Geol. Hydrogeol.* **2021**, *54*, qjegh2020-177. [CrossRef]
9. Wang, L.J.; Guo, M.; Sawada, K.; Lin, J.; Zhang, J. Landslide Susceptibility Mapping in Mizunami City, Japan: A Comparison between Logistic Regression, Bivariate Statistical Analysis and Multivariate Adaptive Regression Spline Models. *CATENA* **2015**, *135*, 271–282. [CrossRef]
10. Wu, Y.; Li, W.; Wang, Q.; Liu, Q.; Yang, D.; Xing, M.; Pei, Y.; Yan, S. Landslide Susceptibility Assessment Using Frequency Ratio, Statistical Index and Certainty Factor Models for the Gangu County, China. *Arab. J. Geosci.* **2016**, *9*, 1–16. [CrossRef]
11. Lv, J.; Zhang, R.; Shama, A.; Hong, R.; He, X.; Wu, R.; Bao, X.; Liu, G. Exploring the Spatial Patterns of Landslide Susceptibility Assessment Using Interpretable Shapley Method: Mechanisms of Landslide Formation in the Sichuan-Tibet Region. *J. Environ. Manag.* **2024**, *366*, 121921. [CrossRef]
12. Catani, F.; Lagomarsino, D.; Segoni, S.; Tofani, V. Landslide Susceptibility Estimation by Random Forests Technique: Sensitivity and Scaling Issues. *Nat. Hazards Earth Syst. Sci.* **2013**, *13*, 2815–2831. [CrossRef]
13. Pourghasemi, H.R.; Sadhasivam, N.; Amiri, M.; Eskandari, S.; Santosh, M. Landslide Susceptibility Assessment and Mapping Using State-of-the Art Machine Learning Techniques. *Nat. Hazards* **2021**, *108*, 1291–1316. [CrossRef]
14. Ullah, M.; Tang, B.; Huangfu, W.; Yang, D.; Wei, Y.; Qiu, H. Machine Learning-Driven Landslide Susceptibility Mapping in the Himalayan China–Pakistan Economic Corridor Region. *Land* **2024**, *13*, 1011. [CrossRef]

15. Sun, D.; Gu, Q.; Wen, H.; Xu, J.; Zhang, Y.; Shi, S.; Xue, M.; Zhou, X. Assessment of Landslide Susceptibility along Mountain Highways Based on Different Machine Learning Algorithms and Mapping Units by Hybrid Factors Screening and Sample Optimization. *Gondwana Res.* **2023**, *123*, 89–106. [CrossRef]
16. Lee, S.M.; Lee, S.J. Landslide Susceptibility Assessment of South Korea Using Stacking Ensemble Machine Learning. *Geoenviron. Disasters* **2024**, *11*, 7. [CrossRef]
17. Wang, Y.; Fang, Z.; Wang, M.; Peng, L.; Hong, H. Comparative Study of Landslide Susceptibility Mapping with Different Recurrent Neural Networks. *Comput. Geosci.* **2020**, *138*, 104445. [CrossRef]
18. Wakjira, T.G.; Alam, M.S. Performance-Based Seismic Design of Ultra-High-Performance Concrete (UHPC) Bridge Columns with Design Example—Powered by Explainable Machine Learning Model. *Eng. Struct.* **2024**, *314*, 118346. [CrossRef]
19. Sundararajan, K.; Srinivasan, K. A Synergistic Optimization Algorithm with Attribute and Instance Weighting Approach for Effective Drought Prediction in Tamil Nadu. *Sustainability* **2024**, *16*, 2936. [CrossRef]
20. Mohamed, N.A.; Hasanien, H.M.; Alkuhayli, A.; Akmaral, T.; Jurado, F.; Badr, A.O. Hybrid Particle Swarm and Gravitational Search Algorithm-Based Optimal Fractional Order PID Control Scheme for Performance Enhancement of Offshore Wind Farms. *Sustainability* **2023**, *15*, 11912. [CrossRef]
21. *ESRI ArcMap*, version 10.3; ESRI: Redlands, CA, USA, 2016.
22. Pham, B.T.; Luu, C.; Van Phong, T.; Trinh, P.T.; Shirzadi, A.; Renoud, S.; Asadi, S.; Van Le, H.; von Meding, J.; Clague, J.J. Can Deep Learning Algorithms Outperform Benchmark Machine Learning Algorithms in Flood Susceptibility Modeling? *J. Hydrol.* **2021**, *592*, 125615. [CrossRef]
23. Tehrany, M.S.; Jones, S.; Shabani, F. Identifying the Essential Flood Conditioning Factors for Flood Prone Area Mapping Using Machine Learning Techniques. *CATENA* **2019**, *175*, 174–192. [CrossRef]
24. Taylor, R.A.; Pare, J.R.; Venkatesh, A.K.; Mowafi, H.; Melnick, E.R.; Fleischman, W.; Hall, M.K. Prediction of In-hospital Mortality in Emergency Department Patients With Sepsis: A Local Big Data–Driven, Machine Learning Approach. *Acad. Emerg. Med.* **2016**, *23*, 269–278. [CrossRef] [PubMed]
25. Loecher, M. Unbiased Variable Importance for Random Forests. *Commun. Stat.—Theory Methods* **2020**, *51*, 1413–1425. [CrossRef]
26. Karaboga, D. *An Idea Based on Honey Bee Swarm for Numerical Optimization*; Erciyes University, Engineering Faculty, Computer Engineering Department: Kayseri, Turkey, 2005.
27. Kaya, E.; Gorkemli, B.; Akay, B.; Karaboga, D. A Review on the Studies Employing Artificial Bee Colony Algorithm to Solve Combinatorial Optimization Problems. *Eng. Appl. Artif. Intell.* **2022**, *115*, 105311. [CrossRef]
28. Wang, H.; Wang, W.; Xiao, S.; Cui, Z.; Xu, M.; Zhou, X. Improving Artificial Bee Colony Algorithm Using a New Neighborhood Selection Mechanism. *Inf. Sci.* **2020**, *527*, 227–240. [CrossRef]
29. Öztürk, Ş.; Ahmad, R.; Akhtar, N. Variants of Artificial Bee Colony Algorithm and Its Applications in Medical Image Processing. *Appl. Soft Comput. J.* **2020**, *97*, 106799. [CrossRef]
30. Cao, M.-T.; Cheng, M.-Y.; Wu, Y.-W. Hybrid Computational Model for Forecasting Taiwan Construction Cost Index. *J. Constr. Eng. Manag.* **2015**, *141*, 04014089. [CrossRef]
31. Wakjira, T.G.; Abushanab, A.; Alam, M.S. Hybrid Machine Learning Model and Predictive Equations for Compressive Stress-Strain Constitutive Modelling of Confined Ultra-High-Performance Concrete (UHPC) with Normal-Strength Steel and High-Strength Steel Spirals. *Eng. Struct.* **2024**, *304*, 117633. [CrossRef]
32. Wakjira, T.G.; Alam, M.S. Peak and Ultimate Stress-Strain Model of Confined Ultra-High-Performance Concrete (UHPC) Using Hybrid Machine Learning Model with Conditional Tabular Generative Adversarial Network. *Appl. Soft Comput.* **2024**, *154*, 111353. [CrossRef]
33. Azadeh, A.; Rouzbahman, M.; Saberi, M.; Valianpour, F.; Keramati, A. Improved Prediction of Mental Workload versus HSE and Ergonomics Factors by an Adaptive Intelligent Algorithm. *Saf. Sci.* **2013**, *58*, 59–75. [CrossRef]
34. Rico-Juan, J.R.; de La Paz, P.T. Machine Learning with Explainability or Spatial Hedonics Tools? An Analysis of the Asking Prices in the Housing Market in Alicante, Spain. *Expert Syst. Appl.* **2021**, *171*, 114590. [CrossRef]
35. Alexander Dekhtyar CSC 466: Knowledge Discovery From Data Fall 2019. Available online: http://users.csc.calpoly.edu/~dekhtyar/560-Fall2009/lectures/lec09.466.pdf (accessed on 13 August 2021).
36. Cortes, C.; Vapnik, V. Support Vector Networks. *Mach. Learn.* **1995**, *20*, 293–297. [CrossRef]
37. Mahmoodzadeh, A.; Mohammadi, M.; Hashim Ibrahim, H.; Gharrib Noori, K.M.; Nariman Abdulhamid, S.; Farid Hama Ali, H. Forecasting Sidewall Displacement of Underground Caverns Using Machine Learning Techniques. *Autom. Constr.* **2021**, *123*, 103530. [CrossRef]
38. Pan, Y.; Zhang, L. BIM Log Mining: Learning and Predicting Design Commands. *Autom. Constr.* **2020**, *112*, 103107. [CrossRef]
39. Friedman, J.H. Stochastic Gradient Boosting. *Comput. Stat. Data Anal.* **2002**, *38*, 367–378. [CrossRef]
40. Ke, G.; Meng, Q.; Finley, T.; Wang, T.; Chen, W.; Ma, W.; Ye, Q.; Liu, T.Y. LightGBM: A Highly Efficient Gradient Boosting Decision Tree. *Adv. Neural Inf. Process Syst.* **2017**, *30*, 3147–3155.
41. Bentéjac, C.; Csörgő, A.; Martínez-Muñoz, G. A Comparative Analysis of Gradient Boosting Algorithms. *Artif. Intell. Rev.* **2021**, *54*, 1937–1967. [CrossRef]
42. Kutty, A.A.; Wakjira, T.G.; Kucukvar, M.; Abdella, G.M.; Onat, N.C. Urban Resilience and Livability Performance of European Smart Cities: A Novel Machine Learning Approach. *J. Clean. Prod.* **2022**, *378*, 134203. [CrossRef]

43. Shapley, L.S. *A Value for N-Person Games. Contributions to the Theory of Games*; Dover: Mineola, NY, USA, 1953; Volume 2, pp. 307–317.
44. Lundberg, S.M.; Lee, S.I. A Unified Approach to Interpreting Model Predictions. In Proceedings of the Advances in Neural Information Processing Systems 30: Annual Conference on Neural Information Processing Systems 2017, Long Beach, CA, USA, 4–9 December 2017; pp. 4766–4775.
45. Wakjira, T.G.; Ibrahim, M.; Ebead, U.; Alam, M.S. Explainable Machine Learning Model and Reliability Analysis for Flexural Capacity Prediction of RC Beams Strengthened in Flexure with FRCM. *Eng. Struct.* **2022**, *255*, 113903. [CrossRef]
46. Camera, C.A.S.; Bajni, G.; Corno, I.; Raffa, M.; Stevenazzi, S.; Apuani, T. Introducing Intense Rainfall and Snowmelt Variables to Implement a Process-Related Non-Stationary Shallow Landslide Susceptibility Analysis. *Sci. Total Environ.* **2021**, *786*, 147360. [CrossRef]
47. Araújo, J.R.; Ramos, A.M.; Soares, P.M.M.; Melo, R.; Oliveira, S.C.; Trigo, R.M. Impact of Extreme Rainfall Events on Landslide Activity in Portugal under Climate Change Scenarios. *Landslides* **2022**, *19*, 2279–2293. [CrossRef]
48. Qi, S.; Xu, Q.; Lan, H.; Zhang, B.; Liu, J. Spatial Distribution Analysis of Landslides Triggered by 2008.5.12 Wenchuan Earthquake, China. *Eng. Geol.* **2010**, *116*, 95–108. [CrossRef]
49. Zhao, S.; Zhao, Z. A Comparative Study of Landslide Susceptibility Mapping Using SVM and PSO-SVM Models Based on Grid and Slope Units. *Math. Probl. Eng.* **2021**, *2021*, 8854606. [CrossRef]
50. Cui, Y.; Jin, J.; Huang, Q.; Yuan, K.; Xu, C. A Data-Driven Model for Spatial Shallow Landslide Probability of Occurrence Due to a Typhoon in Ningguo City, Anhui Province, China. *Forests* **2022**, *13*, 732. [CrossRef]
51. Huang, F.; Tao, S.; Chang, Z.; Huang, J.; Fan, X.; Jiang, S.-H.; Li, W. Efficient and Automatic Extraction of Slope Units Based on Multi-Scale Segmentation Method for Landslide Assessments. *Landslides* **2021**, *18*, 3715–3731. [CrossRef]
52. Chen, X.; Chen, J.; Cui, P.; You, Y.; Hu, K.; Yang, Z.; Zhang, W.; Li, X.; Wu, Y. Assessment of Prospective Hazards Resulting from the 2017 Earthquake at the World Heritage Site Jiuzhaigou Valley, Sichuan, China. *J. Mt. Sci.* **2018**, *15*, 779–792. [CrossRef]
53. Zou, Q.; Jiang, H.; Cui, P.; Zhou, B.; Jiang, Y.; Qin, M.; Liu, Y.; Li, C. A New Approach to Assess Landslide Susceptibility Based on Slope Failure Mechanisms. *CATENA* **2021**, *204*, 105388. [CrossRef]

Disclaimer/Publisher's Note: The statements, opinions and data contained in all publications are solely those of the individual author(s) and contributor(s) and not of MDPI and/or the editor(s). MDPI and/or the editor(s) disclaim responsibility for any injury to people or property resulting from any ideas, methods, instructions or products referred to in the content.